

What controls the ionized gas turbulent motions in dwarf galaxies?

Alexei V. Moiseev^{1*}, Anton V. Tikhonov^{2†}, and Anatoly Klypin³

¹*Special Astrophysical Observatory, Russian Academy of Sciences‡, 369167 Nizhniĭ Arkhyz, Karachaevo-Cherkesskaya Republic, Russia*

²*St. Petersburg State University, Universitetskii pr. 28, 198504 St. Petersburg, Stary Peterhof, Russia*

³*New Mexico State University, USA*

Accepted Received

ABSTRACT

Using 3D spectroscopy with a scanning Fabry–Perot interferometer, we study the ionized gas kinematics in 59 nearby dwarf galaxies. Combining our results with data from literature, we provide a global relation between the gas velocity dispersion σ and the star formation rate (SFR) and $H\alpha$ luminosity for galaxies in a very broad range of star formation rates $SFR=0.001 - 300 M_{\odot} \text{ yr}^{-1}$. We find that the $SFR - \sigma$ relation for the combined sample of dwarf galaxies, star forming, local luminous, and ultra-luminous infrared galaxies can be fitted as $\sigma \propto SFR^{5.3 \pm 0.2}$. This implies that the slope of the $L - \sigma$ relation inferred from the sample of rotation supported disc galaxies (including mergers) is similar to the $L - \sigma$ relation of individual giant HII regions. We present arguments that the velocity dispersion of the ionized gas does not reflect the virial motions in the gravitational potential of dwarf galaxies, and instead is mainly determined by the energy injected into the interstellar medium by the ongoing star formation.

Key words: galaxies: dwarf – galaxies: kinematics and dynamics – galaxies: ISM – ISM: bubbles.

1 INTRODUCTION

The nature of high-velocity turbulent motions of ionized gas in giant star-forming regions and dwarf galaxies has been studied for almost half a century, starting with Smith & Weedman (1970), who showed that the velocity dispersion, σ (the rms velocity along line-of-sight) in giant star forming regions of the M33 and M101 galaxies, determined from the width of the integral $H\alpha$ emission line profiles is about a few tens of km s^{-1} . A close correlation was later found between the rms velocity σ , the diameter, and the total Balmer line luminosity (in the $H\beta$ emission line) of the emitting nebula (Melnick 1977; Terlevich & Melnick 1981). Similar trends were found for individual HII regions and for dwarf irregular (dIrr) and blue compact (BCDG or HII) galaxies. Because of the tightness of the observed $L(H\beta) - \sigma$ relation of star-bursting compact galaxies, it was proposed as an independent indicator of the cosmological distance (e.g. Melnick et al. 1987, 2000; Chávez et al. 2012; Koulouridis, et al. 2013; Chávez et al. 2014).

Relation between the emission-line luminosity L and

ionized gas σ is also important for understanding how star formation affects motion of gas and how star formation is regulated by different stellar feedback processes. Although the existence of a close correlation between these quantities has been known for a long time, the origin of luminosity–velocity dispersion relation in HII galaxies and giant HII regions remains unclear (Terlevich & Melnick 1981; Chu & Kennicutt 1994; Scalo & Chappell 1999; Bordalo et al. 2009; Moiseev & Lozinskaya 2012). The following factors may affect the width of the observed ionized hydrogen lines:

(i) Thermal broadening, which amounts to $\sigma_{th} \approx 8 - 10 \text{ km s}^{-1}$ for typical electron temperatures in the HII regions 7 000–10 000 K.

(ii) Turbulent motions determined by the combined influence of young stellar clusters on the interstellar medium (ISM).

(iii) Gravitational broadening, caused by virial motions of gas clouds in galaxy gravitational potential.

(iv) Non-virial gravitational motions: ISM turbulence associated with tidal interactions, galaxy merging and external gas accretion (e.g. numerical simulations by Bournaud et al. (2011), observational constrains in Arribas et al. (2014) and references therein.)

* moisev@gmail.com

† Deceased

‡ The system of Russian Academy of Sciences institutes was liquidated on Sep 2013

When presenting and discussing the $L - \sigma$ relation, we will always assume, except in specially mentioned cases, that L is the total luminosity of a galaxy or a HII region in the $H\alpha$ line, and σ is the average (luminosity-weighted) velocity dispersion of ionized gas.

It is often assumed that the gravitational effects are the dominant factor in giant HII regions and HII galaxies (e.g., Terlevich & Melnick 1981; Tenorio-Tagle et al. 1993; Melnick et al. 1987). The main argument was that the velocity dispersion of ionized gas is largely determined by the wind of stars that participate in virial motions with the characteristic velocity σ_{stars} . Then σ and σ_{stars} are mainly controlled by the gravitational potential of the object, and the $L - \sigma$ relation is similar to the Faber-Jackson relation for elliptical galaxies: $L \propto \sigma_{\text{stars}}^4$. Different studies of the ionized gas kinematics in giant extragalactic HII regions give a value between ~ 3 and ~ 7 for the exponent in the $L - \sigma$ relation (Blasco-Herrera et al. 2010, 2013). Chávez et al. (2014) present a detailed analysis of this relation for a sample of 128 local compact HII galaxies. They demonstrate that adding the second (the size of HII regions) or even the third (the emission line equivalent width EW or the continuum color and metallicity) parameters significantly improve the correlation. They also argue in favor of the gravitational origin of the ionized gas velocity dispersion σ . They also emphasize that in order the $L - \sigma$ to be tight, the regions of recent bursts of star formation should be gravitationally bound, compact, massive, and have strong emission lines with $EW(H\beta) > 50\text{\AA}$ with pure Gaussian profile without any evidences of multiplicity or rotation.

A different view on the $L - \sigma$ relation was developed beginning with Gallagher & Hunter (1983), who suggested that the processes related with the energy of embedded OB stars drive the ionized gas velocity dispersion in giant HII regions on scales smaller than 0.5 kpc, while properties of larger supergiant HII complexes agree with a gravitationally driven σ . Based on Fabry-Perot interferometric observations of nearby galaxies Arsenault & Roy (1988) also concluded that effects of stellar wind and turbulence are more important for the kinematics of giant HII regions compared with virial motions. There are different ways of how a young stellar population affects the surrounding ISM. According Mac Low & Klessen (2004), (see also Lopez et al. 2014, and references therein) the main mechanisms are: protostellar outflows, stellar winds and ionizing radiation pressure of massive stars, supernovae (SN) explosions, the dust-processed infrared radiation, and warm and hot gas pressure. The contribution of different factors changes with spatial and density scale. For instance, Lopez et al. (2014) found that warm ionized gas dominates over the other terms of pressure in all considered HII regions in Large and Small Magellanic Clouds. Numerical simulations also demonstrate that the radiation pressure is a very important feedback mechanism for models of formation of galaxies compared with the hot gas contribution (heated by SNs and stellar winds) (e.g., Hopkins et al. 2012; Ceverino et al. 2014; Trujillo-Gomez et al. 2015). Note that together with the chaotic gas motions, responsible for the Gaussian emission line profile, the effects related with individual expanding shells may lead to the appearance of non-symmetric features such as wings and peaks in the line profile (see examples in

Melnick, Tenorio-Tagle & Terlevich 1999; Bordalo & Telles 2011).

Some recent observations also provide evidence that energy injected into the interstellar medium by the ongoing star formation process is the main factor affecting gas turbulent motions. For example, Green et al. (2010) show that in a wide range of galaxy luminosities the ionized gas rms velocity σ is determined by the star formation rate (SFR), which is proportional to the $H\alpha$ luminosity, and does not correlate with the galaxy mass. Earlier, Dib, Bell & Burkert (2006) showed that σ for neutral gas also depends on the SFR. However other numerical simulations with higher resolution in a stratified ISM suggested that this trend is absent if the gas surface density increases with the SN rate (Joung et al. 2009). On the other hand, the galaxy-scale simulations that included stellar feedback (Hopkins et al. 2012) clearly demonstrate that the average velocity dispersion of the gas (in all cold, warm and hot phases) increases with the total SFR. Also, Dopita (2008) argues that kinetic energy of ionized gas in the star formation regions is proportional to the local SFR, integrated over the duration of the burst. Moiseev & Lozinskaya (2012) demonstrate a close correlation between the two-dimensional distribution of the radial velocity dispersion of ionized gas and the surface brightness in the $H\alpha$ line for a sample of nearby dwarf galaxies: most of the regions with the highest velocity dispersion belong to a low-brightness diffuse background surrounding large HII-regions. Recent simulations of multiple SN explosions were able to reproduce the diagrams ‘ $H\alpha$ intensity – velocity dispersion’ observed in these galaxies when a realistic spatial resolution was used (Vasiliev, Moiseev & Shchekinov 2015).

However, some other recent studies of high-redshift galaxies contradict Green et al. (2010). For instance, integral-field data by Genzel et al. (2011) demonstrate a very weak correlation of σ and SFR density for star-forming clumps in galaxies at $z = 2.2 - 2.4$. Further Wisnioski et al. (2012) and Swinbank et al. (2012) using observations with similar technique argue that such clumps follow the same $L - \sigma$ relation as gravitational bounded local giant HII regions according Terlevich & Melnick (1981) and related studies.

To summarize, the question of the nature of high-velocity turbulent motions of ionized gas in dwarf galaxies still remains open. One of the problems is the lack of sufficiently uniform observational data. Recent results by Bordalo & Telles (2011) fill this gap to a certain extent. They give a uniform set of high-resolution spectroscopy observations for 118 star formation regions in HII galaxies. Chávez et al. (2014) presented similar data for 128 HII galaxies selected from the SDSS. They also discussed the impact of other factors (gas metallicity, ionization state, the history of star formation) on the $L - \sigma$ relation.

However, most of the results are based on slit spectroscopy. The distribution of ionized gas in dwarf galaxies has a complex irregular morphology, and the two-dimensional velocity dispersion maps, obtained using the 3D spectroscopy can provide the most complete information about gas turbulence.

The second important issue is related with the fact that the luminosity-weighted velocity dispersion has become a widely used value to characterize the turbulent gas motions

in samples of distant and nearby galaxies (Östlin et al. 2001; Green et al. 2010; Davies et al. 2011; Blasco-Herrera et al. 2013; Arribas et al. 2014). How does the $L-\sigma$ relation work for galaxies of different types and luminosities? Do galaxies obey the same scaling relation as the HII regions and star forming clumps?

In this paper we analyse ionized gas turbulent motions in 59 galaxies observed at the 6-m Big Telescope Altazimuthal (BTA) of Special Astrophysical Observatory of the Russian Academy of Sciences (SAO RAS) using a scanning Fabry–Perot interferometer (FPI). Most of our sample consists of dwarf galaxies of the Local Universe. Using this unique material, we were able to extend the $L-\sigma$ relation for objects much weaker than in the samples described earlier.

2 OBSERVATIONS AND DATA REDUCTION

2.1 Sample of galaxies

Our sample is based on the archive data of observations at the 6-m telescope of SAO RAS. It consists of several subsamples of galaxies studied within the framework of several observational programs:

- The Local Volume (LV) subsample: 36 nearby dwarf galaxies with galactocentric distances $D < 15$ Mpc. These are mostly low-luminosity objects with the average absolute magnitude $M_B \approx -14$. The ionized gas velocity dispersion maps of 10 galaxies from this subsample were already reported by Moiseev & Lozinskaya (2012).
- The XMD subsample of 9 more distant ($D = 14 - 86$ Mpc) and bright ($M_B \approx -15$) dwarf galaxies with extremely low metallicity, and 2 low surface brightness companion galaxies. Their internal kinematics were described and analysed in Moiseev, Pustilnik & Kniazev (2010b).
- The BCDG subsample: 12 blue compact dwarf galaxies at distances $D = 10 - 78$ Mpc; all are brighter than $M_B = -15$. Some of them (e.g., Mrk 297 or III Zw 102) are sometimes included in BCDG samples (see Cairós et al. 2001), though they cannot be formally called dwarf galaxies since their absolute magnitude is brighter than $M_B = -20$ and the amplitude of the rotation curve exceeds 140 km s^{-1} . The observational data for 3 of these galaxies were presented by Martínez-Delgado et al. (2007).

The full sample consists of 59 galaxies, and covers a wide range of luminosities from $M_B = -11$ to $M_B = -21$. The overwhelming majority (51/59=86 per cents) of them are dwarf galaxies with the absolute magnitudes $M_B > -18$.

The observations were carried out in the prime focus of the 6-m telescope of SAO RAS using a scanning FPI mounted inside the SCORPIO focal reducer (Afanasiev & Moiseev 2005). In 2014 its new version SCORPIO-2 (Afanasiev & Moiseev 2011) was used. The operating spectral range around the $H\alpha$ line was cut using a narrow bandpass filter. About $\sim 2/3$ of the observations were performed using the FPI501 interferometer, providing in the $H\alpha$ emission line a free spectral range between the neighboring interference orders $\Delta\lambda = 13 \text{ \AA}$ and spectral resolution ($FWHM$ of the instrumental profile) of about 0.8 \AA (35 km s^{-1}), sampled by 0.36 \AA per channel. After November 2009 we used a new FPI751 interferometer, which has

$\Delta\lambda = 8.7 \text{ \AA}$ and a spectral resolution of 0.4 \AA (18 km s^{-1}), sampled by 0.21 \AA per channel. The Mrk 33 galaxy was observed in the $[\text{NII}]\lambda 6583$ line, all the others – in the $H\alpha$ line.

In 2003–2014, the detectors were CCD EEV 42-40 and E2V 42-90, given the image scale of $0.71 \text{ arcsec pixel}^{-1}$ in the on-chip binned 4×4 mode. In 2002 the TK1024 CCD was used, yielding the scale of $0.56 \text{ arcsec pixel}^{-1}$ in the 2×2 binning mode.

During the scanning process we have consistently obtained 36 interferograms (40 for FPI751) at different distances between the FPI plates. The seeing on different nights varied from 1 to 4 arcsec. The reduction of observational data was performed using the software package running in the IDL environment (Moiseev 2002; Moiseev & Egorov 2008). Following the primary reduction, airglow lines subtraction, photometric and seeing corrections using the reference stars and wavelength calibration, the observational data were combined into the data cubes, where each pixel in the field of view contains a 36- or 40-channel spectrum.

The log of observations is shown in Table 1, listing the galaxy name; the date of observations; the interferometer type; exposure time; the resulting angular resolution after smoothing the reduced data cubes with a two-dimensional Gaussian to increase the signal-to-noise ratio in the areas of low surface brightness. Only the information for the Local Volume galaxies and the BCDG subsamples is shown; see the log of observations in Moiseev et al. (2010b) for the XMD subsample.

2.2 Construction of maps and measuring velocity dispersion

We define the velocity dispersion of ionized gas σ as the standard deviation of the Gaussian profile fitted the $H\alpha$ emission line after accounting for the FPI instrumental profile and subtracting the contribution of thermal broadening in the HII regions. The procedure to measure σ is described in detail in Moiseev & Egorov (2008). In short, the observed profiles of the $H\alpha$ line were fitted by the Voigt function, which is a convolution of Lorentzian and Gaussian functions corresponding to the FPI instrumental profile and broadening of observed emission lines respectively. The FWHM of instrumental profile was estimated each night from Lorentzian fitting of the He-Ne-Ar calibration lamp emission scanned with FPI (Moiseev & Egorov 2008). The results of profile fitting were used to construct two-dimensional line-of-sight velocity fields of ionized gas, maps of line-of-sight velocity dispersion, free from the instrumental profile (σ_{obs}) influence, and also the images of galaxies in the $H\alpha$ emission line and in the continuum.

The accuracy of velocity dispersion was estimated from the measurements of the S/N using the relations given in Figure 5 of Moiseev & Egorov (2008). On the σ maps we masked out the regions with a weak signal, where the formal error of velocity dispersion measurements exceeded $10 - 12 \text{ km s}^{-1}$ (which corresponds to $S/N \leq 5$). Emission line intensity maps were constructed even for regions where the signal-to-noise ratio was smaller: $S/N \approx 2 - 3$.

The correction from the measured $\sigma_{i,obs}$ to the final σ_i , where i corresponds to the pixel number, was done according to the relation (Rozas et al. 2000):

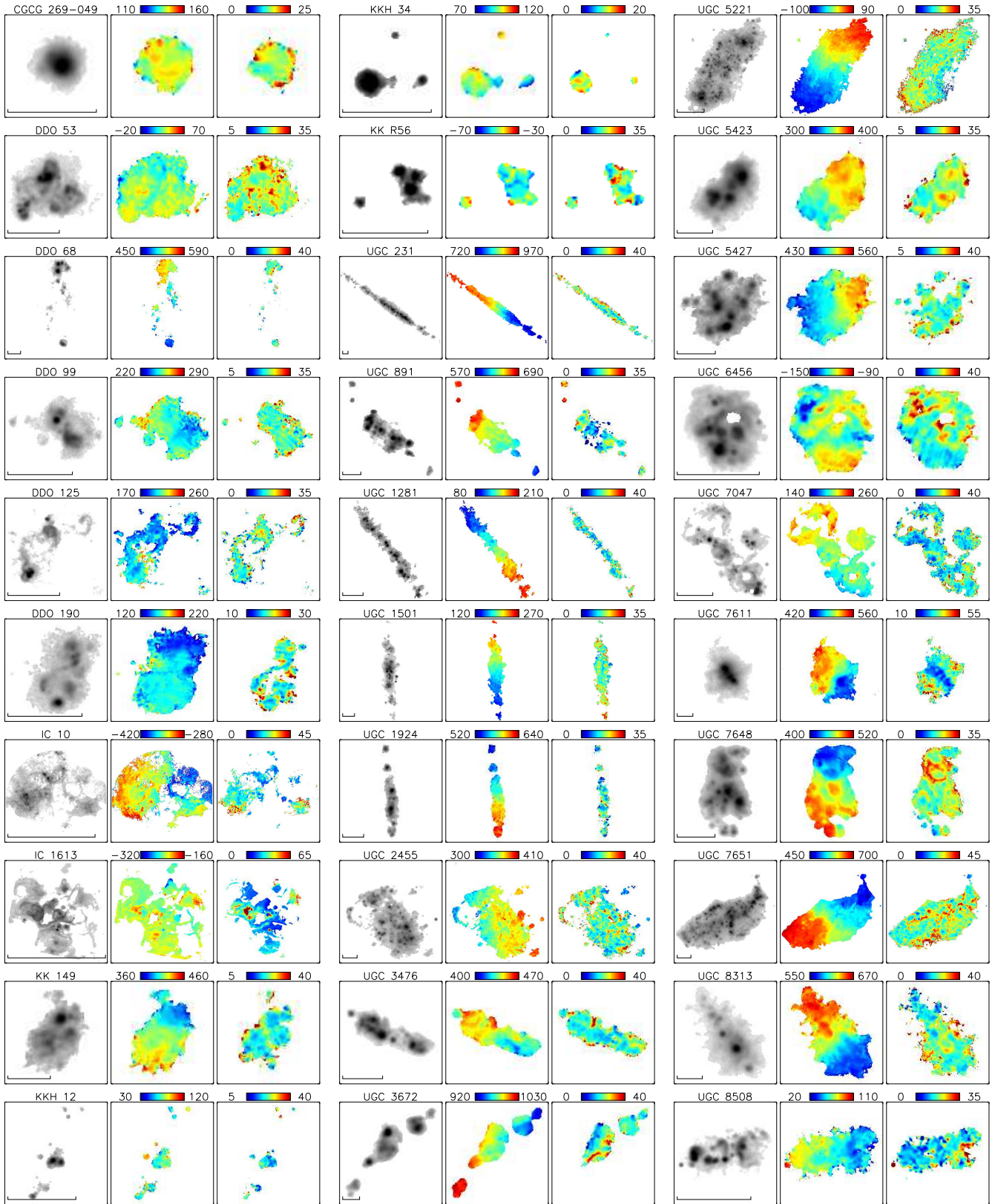


Figure 1. Results of observations with the scanning FPI at the SAO RAS 6-m telescope. Given for each galaxy: an image in the H α line, maps of line-of-sight velocities, and velocity dispersion, corrected for the thermal line broadening. Colour scale is in km s^{-1} . The horizontal bar in the first panel for each galaxy shows the linear scale of 1 kpc.

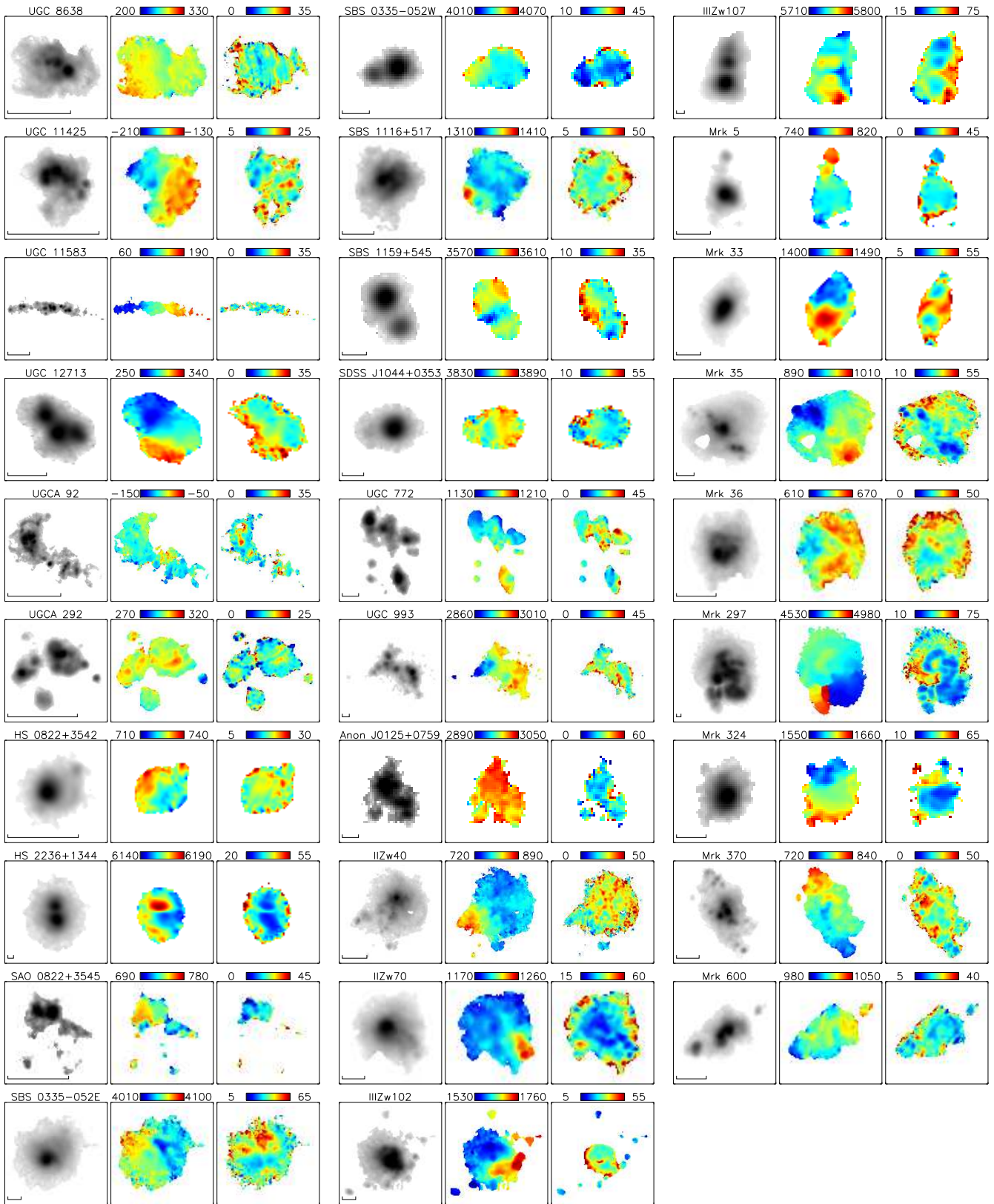


Figure 1. (continue)

Table 1. Log of observations

Name	Date	FPI	Exp. time time (s)	Ang.resol. (arcsec)
Local volume subsample				
CGCG269-049	06.02.2010	FPI751	150 × 40	4.4
DDO 53	26.02.2009	FPI501	200 × 36	3.3
DDO 68	30.12.2006	FPI501	240 × 36	2.7
DDO 99	26.02.2009	FPI501	180 × 36	3.8
DDO 125	18.05.2005	FPI501	180 × 36	3.0
DDO 190	04.03.2009	FPI501	100 × 36	3.3
IC 10	08.09.2005	FPI501	300 × 36	1.2
IC 1613	12.09.2001	FPI501	200 × 36	2.2
KK 149	05.03.2009	FPI501	150 × 36	2.8
KKH 12	23.08.2004	FPI501	120 × 36	2.7
KKH 34	12.11.2009	FPI751	230 × 40	3.4
KKR 56	20.05.2010	FPI751	150 × 40	3.3
UGC 231	11.11.2009	FPI751	200 × 40	2.4
UGC 891	11.11.2009	FPI751	200 × 40	3.1
UGC 1281	14.08.2009	FPI751	110 × 40	2.7
UGC 1501	10.11.2009	FPI751	200 × 40	2.3
UGC 1924	11.11.2009	FPI751	180 × 40	2.3
UGC 3476	02.11.2010	FPI751	220 × 40	2.4
UGC 3672	12.11.2009	FPI751	160 × 40	3.1
UGC 5221	16.12.2014	FPI751	160 × 40	2.0
UGC 5423	26.02.2009	FPI501	180 × 36	3.5
UGC 5427	04.03.2009	FPI501	180 × 36	3.7
UGC 8638	24.02.2009	FPI501	150 × 36	3.9
UGC 6456	29.11.2002	FPI501	300 × 36	2.2
UGC 7611	19.05.2010	FPI751	160 × 40	3.5
UGC 8508	16.05.2005	FPI501	200 × 36	3.0
UGC 11425	14.08.2009	FPI751	140 × 40	3.0
UGC 11583	10.11.2009	FPI751	220 × 40	1.9
UGC 12713	16.05.2005	FPI501	200 × 36	3.0
UGC 2455	07.10.2010	FPI751	240 × 40	2.3
UGC 7047	17-18.03.2012	FPI751	360 × 40	2.2
UGC 7648/51	08.02.2011	FPI751	160 × 40	2.8
UGC 8313	19.03.2012	FPI751	450 × 40	2.7
UGCA 92	10.11.2009	FPI751	180 × 40	2.5
UGCA 292	07.02.2010	FPI751	120 × 40	3.6
BCDG subsample				
II Zw 40	01.12.2003	FPI501	120 × 36	1.9
II Zw 70	30.01.2004	FPI501	180 × 36	2.5
III Zw 107	01.12.2006	FPI501	100 × 36	1.9
III Zw 102	30.11.2003	FPI501	180 × 36	2.7
Mrk 5	30.01.2004	FPI501	240 × 36	2.6
Mrk 33	30.01.2004	FPI501	150 × 36	2.3
Mrk 35	01.12.2003	FPI501	150 × 36	2.1
Mrk 36	29.11.2003	FPI501	160 × 36	1.6
Mrk 297	13.08.2009	FPI751	144 × 40	3.5
Mrk 324	30.11.2003	FPI501	120 × 36	2.8
Mrk 370	30.11.2003	FPI501	120 × 36	2.6
Mrk 600	01.12.2006	FPI501	120 × 36	2.2

$$\sigma_i^2 = \sigma_{i,obs}^2 - \sigma_N^2 - \sigma_{tr}^2, \quad (1)$$

where $\sigma_N \approx 3 \text{ km s}^{-1}$ and $\sigma_{tr} \approx 9.1 \text{ km s}^{-1}$ correspond to the natural width of the emission line and its thermal broadening at the temperature of 10^4 K .

In most of the objects the emission line spectrum is very well described by a single-component Voigt profile. Only a few galaxies have areas where the emission line profile has a complex (usually two-component) structure, showing the presence of expanding shells around the regions of star formation or possible supernova remnants. In

addition to the previously reported cases of UGC 8508, UGCA 92 (Moiseev & Lozinskaya 2012), and SBS 0335-052E (Moiseev et al. 2010b), compact regions with a two-component H α profile were found in UGC 260, UGC 1281, UGC 7047 and UGC 7651.

The mean velocity dispersion for the whole galaxy, weighted with intensity, was calculated as:

$$\sigma = \frac{\sum \sigma_i I_i}{\sum I_i}, \quad (2)$$

Table 2. Integral parameters of galaxies

Name	D Mpc	M_B	M_K	$\log L_{H\alpha}$ erg s $^{-1}$	σ km s $^{-1}$	i deg.	V_{max} km s $^{-1}$
Local volume subsample							
CGCG 269-049	4.59	-13.11	-15.46	37.24	13.6 \pm 1.9	43	9.8
DDO 53	3.56	-13.37	-15.00	38.93	21.0 \pm 1.8	27	16.4
DDO 68	9.80	-15.27	-17.15	39.33	19.9 \pm 3.9	65	57.2
DDO 99	2.64	-13.52	-15.26	38.44	19.2 \pm 2.4	52	11.7
DDO 125	2.74	-14.33	-16.97	38.28	16.3 \pm 2.3	63	17.8
DDO 190	2.80	-14.19	-16.52	38.44	18.5 \pm 2.9	60	24.7
IC 10	0.66	-15.99	-17.90	40.73	17.6 \pm 0.7	31	52.8*
IC 1613	0.73	-14.54	-16.90	38.43	25.9 \pm 1.3	22	26.7*
KK 149	8.90	-14.85	-17.20	38.58	19.0 \pm 4.1	58	26.2
KKH 12	3.00	-13.03	-15.89	38.65	17.9 \pm 4.5	90	19.5*
KKH 34	4.61	-12.30	-14.65	37.18	11.6 \pm 6.6	55	12.8*
KKR 56	5.90	-14.39	-16.74	38.27	17.8 \pm 6.3	–	–
UGC 231	12.82	-18.38	-19.98	39.75	18.0 \pm 3.8	90	92.8
UGC 891	9.38	-15.90	0.00	38.94	15.4 \pm 5.9	65	60.0
UGC 1281	4.97	-16.07	-15.51	39.07	16.7 \pm 5.0	90	56.4
UGC 1501	4.97	-16.52	-18.22	39.52	16.6 \pm 2.4	75	47.5
UGC 1924	9.86	-15.80	-17.41	38.66	14.5 \pm 5.4	90	50.6
UGC 2455	7.80	-18.14	-20.00	40.71	18.3 \pm 2.6	51	47.9
UGC 3476	7.00	-14.27	-16.62	39.22	16.5 \pm 2.3	90	47.3*
UGC 3672	15.10	-13.89	0.00	39.30	18.3 \pm 3.6	56	67.8
UGC 5221	3.56	-17.09	-20.27	40.02	18.1 \pm 1.6	61	58.5*
UGC 5423	8.71	-15.62	-17.74	39.20	22.0 \pm 2.2	56	24.8
UGC 5427	7.10	-14.48	-15.50	38.75	21.3 \pm 4.8	55	54.1
UGC 6456	4.34	-14.03	-15.72	39.23	17.9 \pm 1.3	66	15.0
UGC 7047	4.31	-15.07	-17.42	39.25	15.3 \pm 1.5	46	37.5
UGC 7611	9.59	-17.73	-20.86	40.26	23.1 \pm 2.5	77	51.5
UGC 7648	5.80	-16.72	-18.26	40.01	18.9 \pm 1.8	55	78.1*
UGC 7651	5.80	-19.42	-21.50	40.93	22.8 \pm 1.8	47	129.2
UGC 8313	9.20	-15.22	-17.94	39.58	21.9 \pm 2.0	77	45.0
UGC 8508	2.69	-13.09	-15.58	38.43	13.3 \pm 2.4	51	32.6
UGC 8638	4.27	-13.74	-16.63	38.66	16.1 \pm 1.9	49	18.2*
UGC 11425	3.60	-14.32	-15.57	38.49	14.4 \pm 0.0	35	37.1
UGC 11583	5.90	-14.32	-16.67	38.35	14.6 \pm 4.5	90	46.7
UGC 12713	12.20	-15.95	-16.83	39.45	18.6 \pm 2.2	72	44.9*
UGCA 92	3.01	-15.59	-16.56	39.44	16.5 \pm 3.1	56	39.7*
UGCA 292	3.62	-11.79	-13.56	38.44	11.8 \pm 1.7	45	21.9
XMD subsample							
HS 0822+3542	13.50	-12.90	–	39.24	19.4 \pm 0.7	31	12.3
HS 2236+1344	86.40	-17.04	–	41.02	28.0 \pm 0.9	35	21.8
SAO 0822+3545	13.50	-13.26	–	37.96	17.9 \pm 5.4	63	12.4
SBS 0335-052E	53.80	-16.87	-18.44	41.02	30.6 \pm 1.6	37	28.2
SBS 0335-052W	53.80	-14.68	-16.12	39.70	20.2 \pm 2.7	37	12.4
SBS 1116+517	23.10	-14.73	–	39.97	27.4 \pm 1.5	50	10.4
SBS 1159+545	52.20	-14.65	–	40.24	22.9 \pm 1.3	66	9.1
SDSS J1044+03	53.80	-16.19	–	40.69	28.7 \pm 1.9	51	9.0
UGC 772	16.30	-14.88	–	39.33	22.0 \pm 2.9	40	38.5
UGC 993	40.30	-17.72	–	40.55	22.1 \pm 2.5	69	48.5
Anon J0125+07	40.30	-16.20	–	39.46	25.0 \pm 5.0	64	22.9
BCDG subsample							
II Zw 40	9.69	-18.29	-17.89	41.14	32.5 \pm 1.2	60	50.5
II Zw 70	19.12	-16.56	-18.61	40.47	25.7 \pm 1.2	76	35.0
III Zw 102	22.71	-19.24	-22.91	40.85	31.7 \pm 2.6	60	108.4
III Zw 107	78.09	-19.53	-22.04	41.37	41.1 \pm 1.4	51	25.1
Mrk 5	13.96	-15.47	-18.04	39.55	18.0 \pm 1.6	48	33.5*
Mrk 33	22.30	-18.28	-21.31	40.98	37.7 \pm 2.4	47	32.6
Mrk 35	15.60	-17.76	-20.14	40.43	27.7 \pm 1.2	27	63.6
Mrk 36	10.43	-14.71	-16.14	39.91	23.8 \pm 1.2	47	18.8
Mrk 297	65.10	-21.16	-23.49	41.65	36.7 \pm 1.7	40	121.8
Mrk 324	22.43	-16.44	-18.95	39.68	28.8 \pm 5.1	38	108.0*
Mrk 370	10.85	-16.83	-19.51	40.12	24.9 \pm 2.0	45	53.5
Mrk 600	12.81	-15.43	-17.43	39.78	18.7 \pm 1.6	59	35.5*

 *: V_{max} data from HyperLEDA

where I_i is the observed emission line in the i -th pixel.

Figure 1 presents the results of our observations with the scanning FPI: the image in the $H\alpha$ line, the velocity field, and the velocity dispersion, corrected for the thermal broadening and natural width according eq.(1). The velocity fields usually have more points than the velocity dispersion maps since, at the same S/N level, the velocity is measured with a higher accuracy than the line width.

3 $L - \sigma$ RELATION

The calculated kinematic parameters of the galaxies together with their adopted distances, absolute magnitudes in the B and K_s -bands and total $H\alpha$ luminosity are given in the Table 2. We use the distances, luminosities in the B and K_s -bands, and in the $H\alpha$ emission line for the nearby galaxies provided by the LVG database¹ (Kaisina et al. 2012). All luminosities are corrected for the internal (A_B^i) and Galactic (A_B^g) extinction, according to the values given in this database²

For nearby galaxies not listed in the LVG database (UGC 231, UGC 891, UGC 1924, UGC 3672), the distances were adopted from Karachentsev et al. (2004). For UGC 8313 we use data from Tully (1988). Apparent magnitudes of these galaxies were adopted from RC3 (de Vaucouleurs et al. 1991); the m_K values were retrieved from the 2MASS, A_B^i – according to the relation of Verheijen (2001). The flux in the $H\alpha$ was taken from van Zee (2000) and Kennicutt et al. (2008). Distances and luminosities for the XMD sample were taken – as per Moiseev et al. (2010b), and for the BCDG – from Cairós et al. (2001).

When estimating $L_{H\alpha}$, we take into account the fact that in observations with narrow-band filters authors measure the flux in $H\alpha + [NII]$. The contribution of the nitrogen lines $[NII]\lambda\lambda 6548, 6584$ was determined by an empirical correlation, linking the $[NII]/H\alpha$ ratio with M_B (Kennicutt et al. 2008; Lee et al. 2009). For the most of considered galaxies, fainter than $M_B = -18$ this ratio is small ($[NII]/H\alpha < 0.2$).

The inclination angles i and maximal rotational velocities V_{\max} for the XMD sample are based on the results of Moiseev et al. (2010b). For most of Local Volume galaxies the data are taken from Moiseev (2014). The kinematic parameters of III Zw 102 and UGC 8313 were presented by Moiseev (2008) and Voigtlaender et al. (2015). For other galaxies i and V_{\max} were derived from the ionized gas velocity field in the same manner as described in Moiseev (2014). In cases, where $H\alpha$ rotation curves never clearly come to a plateau, or velocity field of ionized gas are dominated by non-circular motions (objects marked by asterisk in the Table 2), we use estimates from the HyperLeda (Makarov et al. 2014).

The velocity fields shown in Figure 1 reveal a component related with regular rotating discs in a majority of the sample (61 per cents). The fraction of rotation dominated galaxies significantly changes in the different subsamples. In the Local Volume subsample the most of galaxies

(72 per cents or 26 objects) have disc-like ionized gas kinematics. Even among the remaining objects, in some dwarf galaxies (DDO 53, UGC 6456, UGC 8638) appears a component corresponding to a circular rotation. However, in these galaxies non-circular velocities have larger amplitude (Moiseev 2014). In these low-mass galaxies the $H\alpha$ -emitted gas is observed only in the central region, where amplitude of their rotation curve is about $5-10 \text{ km s}^{-1}$. In contrast with the LV subsample, only half of XMD galaxies (55 per cents or 6 objects) demonstrate disc-like rotation gradient, including cases of merger remains (HS 0822+3542 and UGC 772) which reveal two rotating discs with different orientation of spins. This is not surprising because analysis of Moiseev et al. (2010b) provides the evidence for the crucial role of interaction-induced star formation among galaxies in this subsample. The similar situation is also true for BCDG subsample, where only 33 per cents of objects (namely III Zw 102, Mrk 33, Mrk 35 and Mrk 370) show disc-dominated rotation in their velocity fields.

The maps of velocity dispersion σ clearly demonstrate that in the centre of star forming regions the velocity dispersion of ionized gas has a minimum, whereas σ increases towards periphery. Such a feature in the distribution of the ionized gas velocity dispersion was noted earlier in a number of studies (e.g. Moiseev et al. 2010b; Marino et al. 2012) and was discussed in Moiseev & Lozinskaya (2012), where such behavior is attributed to the influence of young stellar groups on the surrounding gas.

Figure 2 shows different variants of $L - \sigma$ dependence for the galaxies in our sample. The literature most often discusses the dependence of σ on $L_{H\alpha}$ (or $L_{H\beta}$), shown in the upper panels. The top left figure separately shows all the three subsamples of galaxies we have observed. It is clear that they form a common sequence without any significant systematic offsets. Given that, the galaxies from the LV in general have a lower luminosity than the XMD and BCDG. For completeness, we present the same data for the nine bright BCDGs from Östlin et al. (1999, 2001) and twelve starburst galaxies from Blasco-Herrera et al. (2013) since the measurement technique used by these authors is completely analogous to ours – averaging of the map of $H\alpha$ velocity dispersion, obtained with a scanning FPI. Their measurements complement our $L_{H\alpha} - \sigma$ sequence in the direction of higher luminosities. Note that we have been able to significantly continue the dependence on $L_{H\alpha} - \sigma$ towards the dwarf galaxies, up to $L_{H\alpha} \propto 10^{37} \text{ erg s}^{-1}$, while the vast majority of papers (Terlevich & Melnick 1981; Bordalo & Telles 2011) considers the HII galaxies with $L_{H\alpha} > 10^{39} \text{ erg s}^{-1}$ (with the exception of papers devoted to various HII regions in the interiors of large galaxies: Arsenault & Roy (1988); Wisnioski et al. (2012), and others). Not to crowd the figures, further on we shall not show separately subsamples nor depict the error bars.

The upper right panel shows the distribution of $L_{H\alpha} - \sigma$ in a more traditional form, on a logarithmic scale along both axes. It can be clearly seen that the dependence between the logarithms of luminosity and dispersion is almost exactly linear with a rather small scatter. This fact was noted in many studies, but, as already mentioned in the Introduction, in the case of giant HII regions it was usually associated with the virial ratio, i.e. by the fact that the ionized gas velocity dispersion is definitely related with stellar velocity dispersion

¹ <http://lv.sao.ru/lvgdb/>

² The absorption in the $H\alpha$ line was assumed to be $0.538(A_B^i + A_B^g)$, and in the K_s -band: $0.085(A_B^i + A_B^g)$.

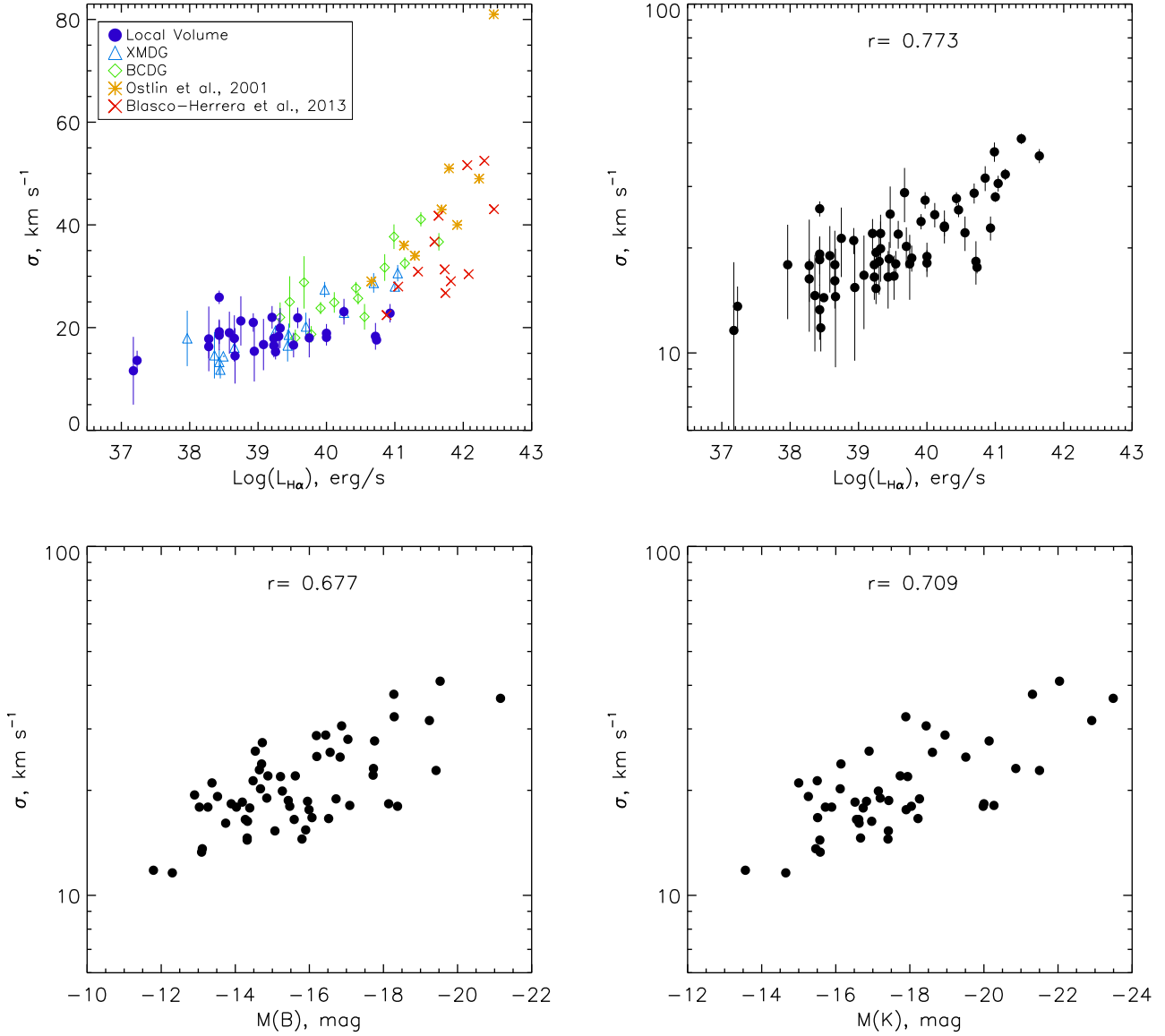


Figure 2. *Top:* The correlation of the average velocity dispersion σ with $H\alpha$ luminosity. *Left:* Linear scale for σ . Color marks different subsamples and data from literature. *Right:* the same plot on the logarithmic vertical scale. Plotted are only the 6-m telescope data. *Bottom:* Dependence of σ on the absolute B (left) and K (right) magnitudes. The correlation coefficient is marked in each panel. Error bars are not shown in the bottom panels to avoid crowding. The velocity σ correlates with the absolute magnitude, but the tightest relation is with the $H\alpha$ luminosity.

and is controlled by the total mass of the system. However, the luminosity in the Balmer emission lines is not a unique function of mass, while it is determined by the number of young OB-stars (Kennicutt 1998, and references therein). While for any reasonable initial stellar mass function, the total stellar mass is determined by the more numerous but less massive stars that can not ionize the surrounding gas. Also the mass of the dark matter correlates exactly with this stellar mass through the Tully-Fisher relation. If σ is defined by the mass of the system, it should better correlate not with $L_{H\alpha}$, but with the luminosity in broader spectral bands, or other parameters that are directly related to the mass.

But this is not observed. Figure 2 shows the $L-\sigma$ dependence, built for M_B . In the optical B -band the older stellar population has a larger contribution, compared to the $H\alpha$ luminosity. However, the point spread here is larger, and the correlation coefficient is smaller: $r = 0.68$ versus $r = 0.77$ in the case of $L_{H\alpha}$. The K -band luminosity is directly related with the total mass of stellar population of the galaxy, moreover, the effect of interstellar reddening is much smaller here. However, the point spread on the $M_K - \sigma$ diagram is same with M_B ($r = 0.71$, Figure 2 bottom right).

We also use a parameter related to the dynamical mass of the system – the amplitude of the rotation velocity, V_{\max} . Left panel in Figure 3 indicates that ionized gas velocity

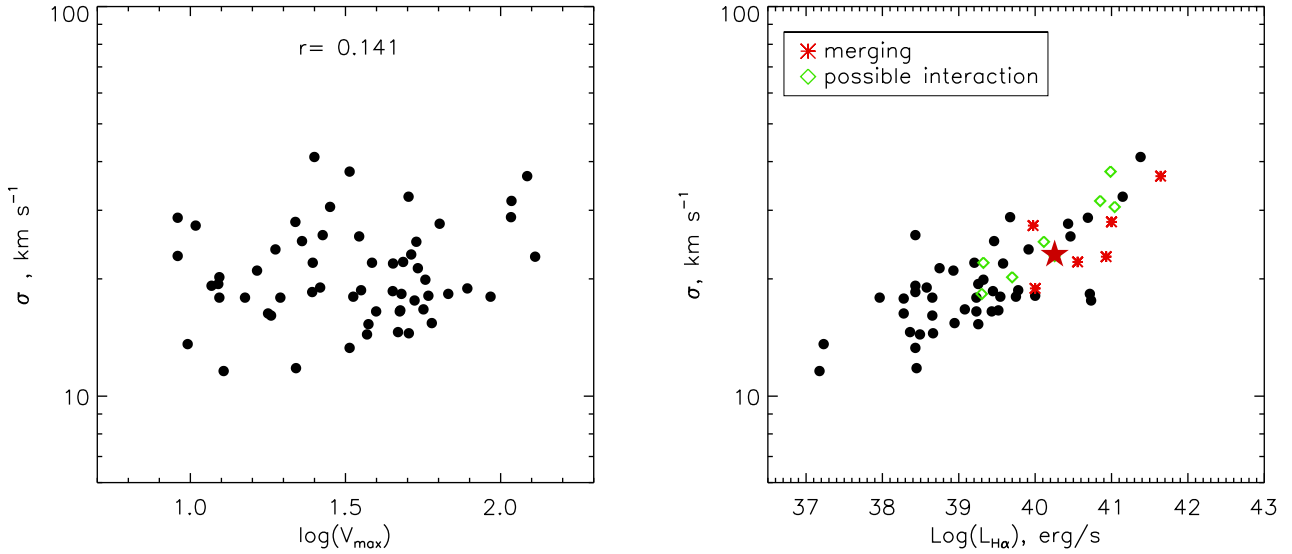


Figure 3. Left: dependence of σ on the amplitude of the rotation curve. Right: the $L_{\text{H}\alpha} - \sigma$ diagram, where the colored dots mark the interacting galaxies. The asterisk shows the superwind galaxy UGC 7611 (NGC 4460).

dispersion does not depend on the amplitude of the rotation velocity V_{max} with the correlation coefficient being very low ($r = 0.14$). For galaxies with $V_{\text{max}} = 10 - 50 \text{ km s}^{-1}$ the gas velocity dispersion is remarkably large. On average $\sigma \approx 20 \text{ km s}^{-1}$ with substantial galaxy-to-galaxy variations. Green et al. (2010) came to a similar conclusion that σ is not related to the total stellar mass for more distant galaxies with violent star formation.

Another argument against a direct relation of σ with the galaxy mass is that there should be observed a systematic departure from the general trend for the galaxies in the transient unrelaxed state, such as merger and interacting. We also attribute to clear mergers such systems as Mrk 297 (two clearly kinematically decoupled components); UGC 993, HS 2236+1344 and SBS 1116+517, where two rotating discs can be identified in the velocity fields (Moiseev et al. 2010b), and a tight pair UGC 7648/7651 (NGC 4485/4490) distorted by interaction. As ‘possible interaction’ galaxies we classify UGC 772, UGC 3672, SBS 0335-052W/E and SBS 1159+545 (see the arguments in Moiseev et al. 2010b) and the galaxies with kinematically decoupled polar components: Mrk 33, Mrk 370 (Moiseev 2011) and IIZw102 (Moiseev 2008). However, in Figure 3 all these galaxies follow a general relationship, just like isolated galaxy UGC 7611 (NGC 4460), where the ionized gas is associated with the circumnuclear star burst and galactic wind outflow (Moiseev et al. 2010a; Moiseev 2014).

Discussed above features of the $L - \sigma$ and $V_{\text{max}} - \sigma$ correlations suggest that the relation between σ and $L_{\text{H}\alpha}$ (i.e. the current SFR) is primary. In this case the correlations of velocity dispersion with M_B , M_L , with the stellar and total mass are secondary, being the consequences of other scaling relations in the galaxies. Indeed, the more massive and bright galaxies with ongoing star formation as a rule tend to have a greater luminosity in the Balmer lines as well.

3.1 Line width σ in dense and diffuse gas

Tenorio-Tagle et al. (1993) used an analytical model to support the idea that σ of ionized gas, observed in giant star-forming regions and HII-galaxies is determined by the mass of these objects. The authors conclude that σ in the regions of greatest brightness (“the kinematic cores of HII-regions”) is directly related to the mass and size of the star forming region. At the same time, bright HII-regions surrounded by the low-brightness coronae of ionized gas with a larger velocity dispersion. Such structure occurs as a result of the influence of young stellar groups on the ISM. But if the velocity dispersion in the centres of star-forming regions determined by the virial motions, then this value – $\sigma(\text{core})$ should be better correlated with the parameters related with mass (M_B , M_K), rather than with $L_{\text{H}\alpha}$, which is controlled by the number of ionizing photons from young massive stars. On the other hand, the average velocity dispersion of diffuse environment should show a clearer (than on the average for the entire galaxy) relation with $L_{\text{H}\alpha}$, since not only the number of Lyman quanta, but also the kinetic energy output of the winds of young stars and supernovae is directly scaled with total number of OB stars (see Figure 1 in Dopita 2008). While the gas velocity dispersion is proportional to the square root of the kinetic energy of turbulent motions.

We separate the velocity dispersion maps into cores of HII regions and a diffuse component. For that we use a histogram of the brightness distribution in the $\text{H}\alpha$ emission line for each galaxy. We consider as belonging to “cores” all the pixels, which contain the top 20 per cents of the total $\text{H}\alpha$ luminosity, while the same 20 percent of the luminosity in the low flux pixels are assigned to the diffuse component. Typical examples of galaxy $\text{H}\alpha$ map separation into two components are shown in Figure 4 that also presents the corresponding histograms of intensity of the surface brightness in $\text{H}\alpha$, explaining the method of separation (the bright and faint tail of the distribution of surface brightness). We

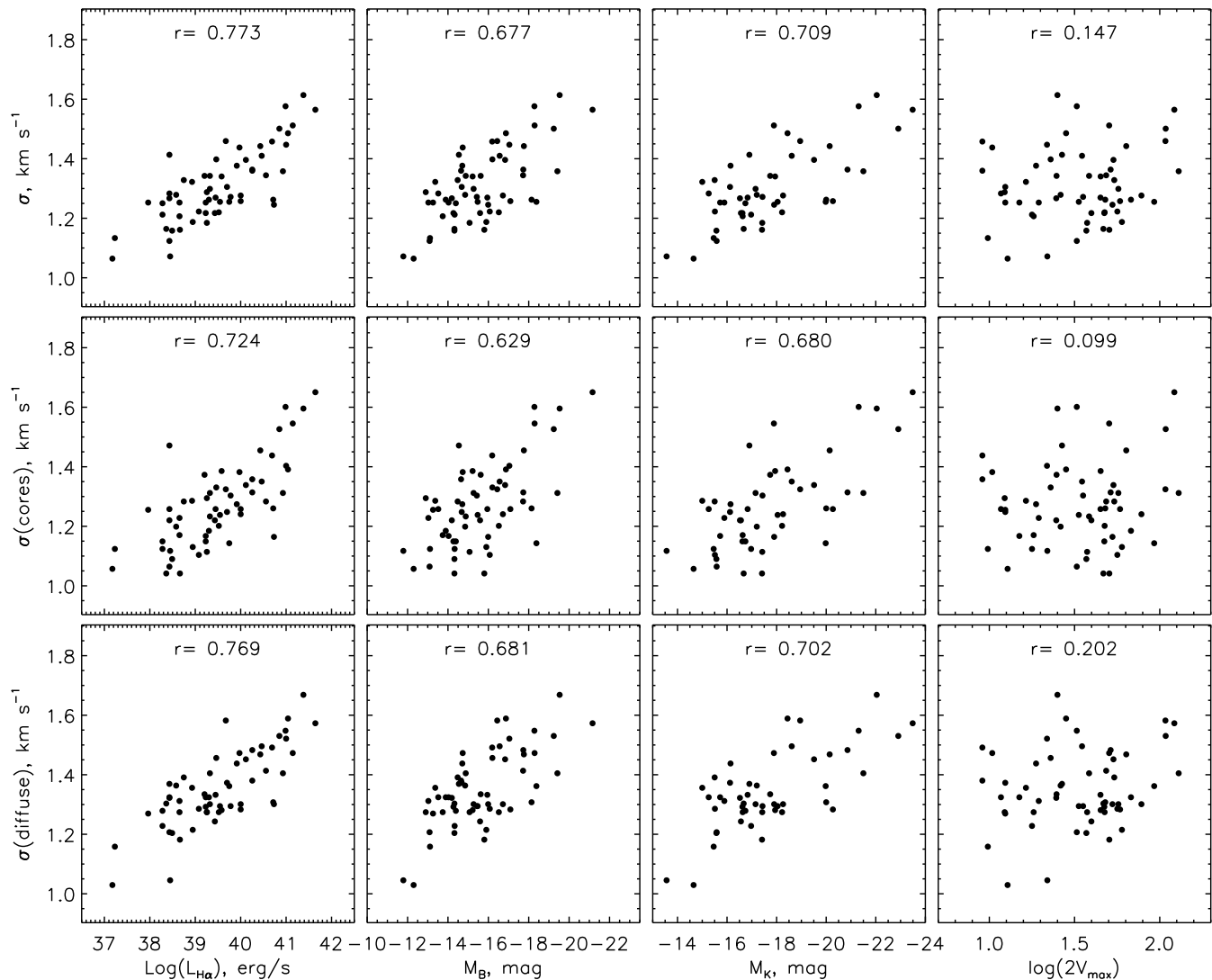


Figure 5. The σ correlations with luminosity in different ranges. Only the galaxies observed with the 6-m telescope. Top: σ was calculated from all pixels of the galaxy image. Middle row: σ was computed only for the cores of star formation regions, where 20 per cents of the total H α luminosity are concentrated. Bottom row: the same for the diffuse component (20 per cents of the total H α luminosity in the low-brightness “tail” in the surface brightness distribution).

can see that “cores” really correspond to the very centres of bright HII regions, while pixels marked as “diffuse” correspond to the envelopes surrounding the regions of star formation.

For each of the components we calculate the flux-weighted velocity dispersion. Figure 5 shows the corresponding relations. It is clear that the gas velocity dispersion of the cores $\sigma(\text{core})$ and of the diffuse component $\sigma(\text{diffuse})$ are very similar. This is also confirmed by the correlation coefficients with respective luminosities that are almost the same, or even lower than those for the σ of the entire disc.

Therefore, the separation into the central and diffuse components shows that the velocity dispersion at the centres of HII regions, as well as the diffuse component are primarily determined by H α luminosity, i.e. by the number of young massive stars. We have performed this analysis for various “core/diffuse” separation criteria. The general conclusion is the same as for the 20 percent criterion described here.

4 GLOBAL $L - \sigma$ AND SFR- σ RELATIONS

As discussed in the Introduction, the $L - \sigma$ relation has been extensively studied, mainly for intergalactic and extragalactic HII regions and compact HII galaxies. All the results agree that there is a power-law relation: $L \propto \sigma^\alpha$. However, the exponent α measured in different studies considerably varies from $\alpha = 3.15$ (Royet et al. 1986) to 6.6 (Hippelein 1986). For discussion see also Blasco-Herrera et al. (2010); Bordalo & Telles (2011); Wisnioski et al. (2012). Recently Chávez et al. (2014) obtained $\alpha = 4.65 \pm 0.14$ using a large sample of compact HII galaxies restricted by velocity dispersion ($\log \sigma < 1.8 \text{ km s}^{-1}$) and equivalent width ($EW(H\beta) > 50 \text{ \AA}$) in order to minimize the contribution of rotation-supported system and/or objects with a complex emission lines structure. Swinbank et al. (2012) suggested $\alpha = 3.8$ which provides a common fit to the both local HII regions and starforming clumps in high-redshift galaxies. It is possible that different flux limits used in observations to

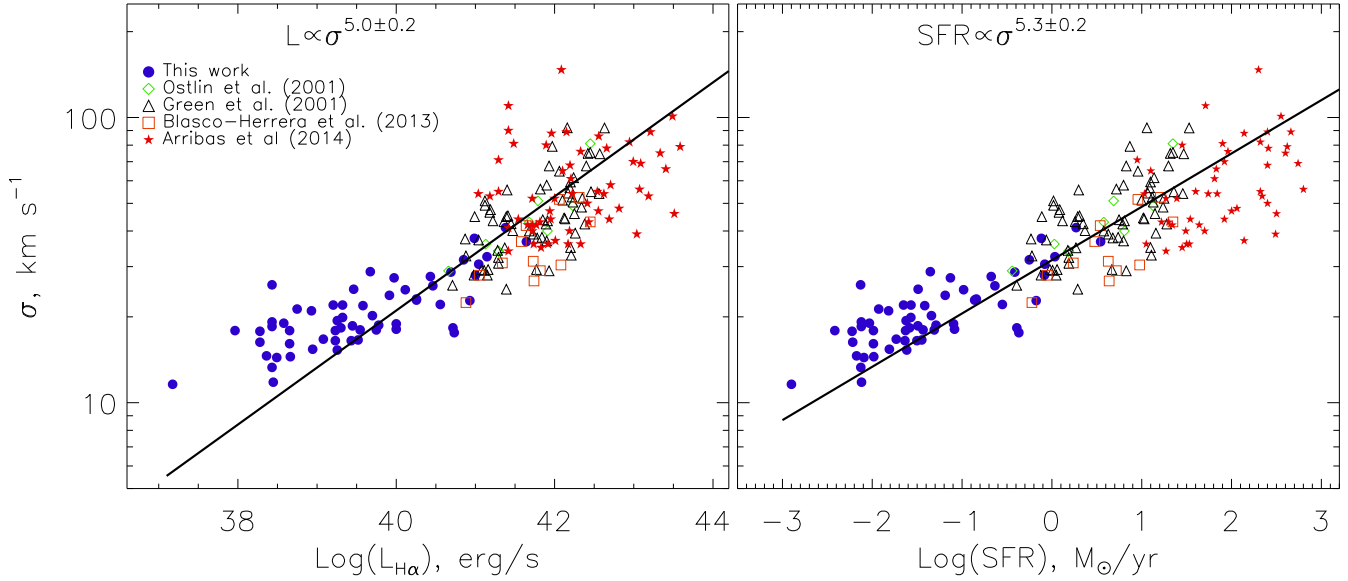


Figure 6. The σ dependence on $H\alpha$ luminosity (left) and on SFR (right) for different types of galaxies. Blue dots depict the galaxies of our sample, the other colors show the 3D-spectroscopic data of other authors for nearby starburst galaxies (see the legend). Black lines show a linear fit of these relationships in different regions.

measure σ for different types of objects (e.g., individual HII regions, dwarf emission galaxies, objects at large redshift) make some contribution to the uncertainty with α . Potential biases of selecting bright $H\alpha$ regions in the long-slit spectroscopy as compared with the full 3D spectroscopy may also contribute to the disagreements. Indeed, Figure 5 shows that the velocity width $\sigma(\text{core})$ in regions with high $H\alpha$ fluxes is systematically smaller than $\sigma(\text{diffuse})$ in regions with low fluxes. If one uses the spectra that are not deep enough, the measured mean velocity dispersion will be underestimated. Another possible reason for the disagreement is that the slope of the $L(\sigma)$ relation changes with the luminosity and with the age of the most recent burst of star formation episode.

Figure 6 combines our measurements with results by other authors who used similar techniques to estimate the ionized gas σ , i.e. 3D-spectroscopic observations (integral-field or scanning FPI) and calculation of the flux-weighted velocity dispersion for the whole galaxy instead individual HII regions: 9 blue compact galaxies from (Östlin et al. 2001), 11 starburst galaxies selected from the SDSS for $z < 0.03$ (Blasco-Herrera et al. 2013), 65 star-forming disc galaxies at $z \sim 0.1$ (Green et al. 2010) and 57 local luminous and ultra-luminous infrared galaxies (U/LIRGSs) without evidences of active galactic nucleus (Arribas et al. 2014). The published data on high-redshift systems were not included because the beam smearing of the velocity gradient can produce a bias in the estimate of the velocity dispersion (Davies et al. 2011).

The figure shows, that for a wide range of luminosities $L_{H\alpha} = 10^{37} - 10^{43.5} \text{ erg s}^{-1}$, there is a tight correlation between $L_{H\alpha}$ and σ . Using the least square fit we derive the slope $\alpha = 5.0 \pm 0.2$ for the present $L - \sigma$ relation ³ This

is why a linear approximation of the $\log L_{H\alpha} - \log \sigma$ relation yields substantially different slopes for large and small luminosities.

Another way of presenting our results is to relate $L_{H\alpha}$ luminosity to the star formation rate SFR. It is known that the $L_{H\alpha}$ luminosity is almost exactly proportional to the rate of ongoing star formation (SFR) of young massive stars (Kennicutt 1998). However, a comparison of SFRs estimated separately from $H\alpha$ data and *GALEX* far-ultraviolet observations shows that for the low luminosities this ratio is broken due to the relative scarcity of massive stars in dwarf galaxies, in relation with their initial mass function. Lee et al. (2009) show that $SFR \propto L_{H\alpha}^{0.62}$ for $L_{H\alpha} < 2.5 \times 10^{39} \text{ erg s}^{-1}$.

The right panel of Figure 6 presents the SFR- σ relation when we use Lee et al. (2009) conversion equations. The full range of the SFR in considered objects is $0.001 - 300 M_{\odot} \text{ yr}^{-1}$. For the U/LIRGSs sample we accepted SFR calculated from the near-infrared (IR) luminosity using an equation from Kennicutt (1998), because a large uncertainties with reddening correction of $L_{H\alpha}$ in these “dusty” systems (Arribas et al. 2014). Indeed, the resulting scatter of points corresponded to the high σ for the SFR seems to be smaller than for the $H\alpha$ luminosities. Note that the combination of the above factors (non-linearity of $SFR - L_{H\alpha}$ relation for the faint dwarf galaxies, and IR-based SFR for the most luminous ULIRGs) leads a linear relation fitted as $SFR \propto \sigma^{5.3 \pm 0.2}$.

Using their data for the U/LIRGSs sample, Arribas et al. (2014) fitted the similar relation as $\sigma \propto SFR^{0.12 \pm 0.03}$ that corresponds to the slope $\alpha = 8.3 \pm 2.1$. This value is significantly larger than our measurements derived for the full sample included both

³ Here σ is considered as an independent variable in agreement with previous studies as it discussed in Bordalo & Telles (2011).

The plots show that there is a sort of kink at $\sim 10^{41} \text{ erg s}^{-1}$, corresponding to $\sigma \sim 30 \text{ km s}^{-1}$.

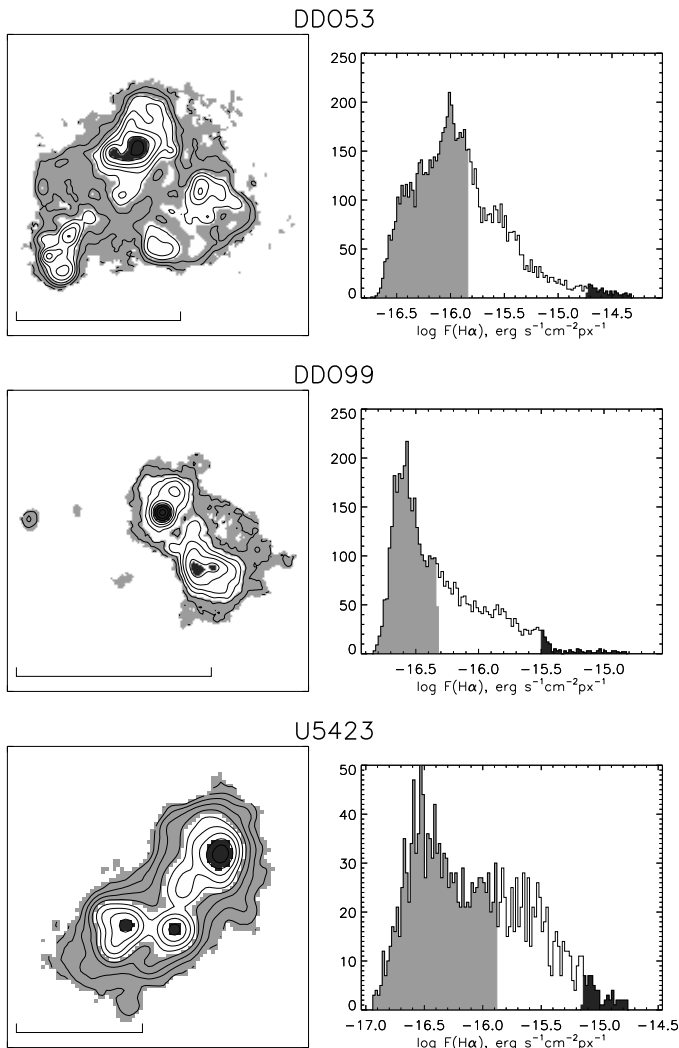


Figure 4. Examples of $H\alpha$ “cores” (regions with very large $H\alpha$ fluxes, dark gray on the maps) and “diffuse” regions (low fluxes, light gray) in DDO53, DDO99 and UGC 5423 galaxies. The isophotes of the $H\alpha$ images are overlaid. The horizontal bar shows the linear scale of 1 kpc. To the right of each map we plot a histogram of the surface brightness distribution of the image pixels in $H\alpha$. The “core” and “diffuse” components are filled with the same shades of gray.

faint and ultra-luminous galaxies. Arribas et al. (2014) suggested that relatively weak dependency of σ on the total SFR , inferred from their fit, is related with the fact that star formation is not a dominant source driving the ionized gas velocity dispersion. Instead, they present arguments in support the scenario where gravitational energy associated with interaction and mergers has a significant contribution to the gas turbulence for the $SFR > 10 M_{\odot} \text{ yr}^{-1}$. However, our results clearly demonstrate the same tendency $SFR - \sigma$ for the dwarf galaxies with and without interaction as well as for U/LIRGs, which appear to have a larger fraction of ongoing mergers. This fact may indicate that the role of interactions in driving ionized gas turbulence in U/LIRGs was overestimated.

The other intriguing fact is that the slope of the $L - \sigma$ relation inferred from our analysis ($\alpha \approx 5.0 - 5.3$) is near the

value $\alpha = 4.7$ obtained by Chávez et al. (2014). From the one hand, Chávez et al. (2014) considered individual giant HII regions and avoided rotation-support system. From the other hand, the most of galaxies presented on Figure 6 reveal a domination of circular rotation discs in their kinematics. In previous sections we presented arguments that the ongoing star formation is a dominant driver of σ calculated for the whole galactic disc. Why are the galaxies of very different types and luminosities follow a similar $L - \sigma$ relation with the systems where “the main mechanism of line broadening is linked to the gravitational potential of the young massive cluster” (Chávez et al. 2014)? Note that the range of luminosities on the relation shown on the Fig. 6 is twice larger as compared with $L - \sigma$ considered in previous works for compact HII galaxies.

5 DISCUSSION

Green et al. (2010) convincingly show that in a wide range of galaxy luminosities, including the objects at $z = 1 - 3$, the mean velocity dispersion σ is determined only by the star formation rate (i.e. by the $H\alpha$ luminosity) and does not correlate with mass. In this case, σ is characteristic of the energy injected in the ISM by stellar winds, supernova explosions, and stellar radiation. For the velocity dispersion of neutral gas, a similar conclusion – weak correlation with galaxy mass – was previously drawn by Dib et al. (2006). Further, the analysis of the shape of integrated HI profiles by Stilp et al. (2013) shows that the velocity dispersion of a broad component of the HI line in dwarf galaxies is defined by the SFR/M_{HI} ratio, although the dependence on the galaxy mass is also present.

Previously we found that there is a close relationship between the two-dimensional distributions of the line-of-sight velocity dispersions of the ionized gas and the local $H\alpha$ luminosity (Moiseev & Lozinskaya 2012). Specifically, we found that most of the areas with the highest velocity dispersion belong to the diffuse low brightness gas, surrounding the star forming regions. This contradicts the idea that σ is determined mainly by the distribution of mass in the of galaxy. In this case one would have expected a different pattern – the maximum of velocity dispersion at the centres of star-forming regions and a decreasing σ with the distance from the centre.

In the present paper we discuss different types of correlations of σ with integral parameters of galaxies – the amplitude of the rotation curve, and luminosities in different bands. We find that the relationship with the parameters characterizing the mass of the galaxy is considerably less distinct than the one with the ongoing star formation, determined by the $H\alpha$ luminosity. Moreover, the current SFR determines the magnitude of supersonic turbulent motions of gas not only in the starburst galaxies, but also in objects with a very low SFR up to $10^{-3} M_{\odot} \text{ yr}^{-1}$.

We analyse two-dimensional velocity fields of ionized gas using observations at the 6-m BTA telescope. This allows us to confidently measure the mean σ across a galaxy, and study details of its distribution inside and outside of star-forming regions. Our new data significantly extend the published $L - \sigma$ relations to the low mass galaxies and pro-

vide the observational evidence that the star formation determines the velocity dispersion of the ionized gas:

- The ionized gas velocity dispersion, luminosity-averaged across the galaxy, is better correlated with the luminosity in the $H\alpha$ line than in the broad B and K -bands. There is almost no correlation of the velocity dispersion σ with the rotation velocity of galaxy.

- The gas velocity dispersion σ in the cores of star-forming regions is nearly the same as σ in the diffuse component with low $H\alpha$ fluxes.

- There a common $SFR-\sigma$ relation for the local galaxies in a very broad range of luminosities $L_{H\alpha} = 10^{37} - 10^{43.5}$ that corresponds $SFR = 0.001 - 300 M_{\odot} \text{ yr}^{-1}$. The fit of this relation $\sigma \propto SFR^{\alpha}$ provides the slope $\alpha = 5.3 \pm 0.2$.

We therefore conclude that velocity of turbulent motions of ionized gas in galaxies is defined mainly by the energy that is transferred to the interstellar medium from young stellar populations in the form of ionizing radiation pressure, and by the winds of young stars and supernova explosions. We believe that this conclusion is important for both simulations of galaxy formation and for interpretation of the apparent emission line widths in galaxies affected by various processes (e.g., star formation, merging, and virial motions).

ACKNOWLEDGMENTS

We are very grateful to the anonymous referee, and to Santiago Arribas, Eduardo Telles and Roberto Terlevich for their constructive comments and suggestions that helped us to improve and clarify our result. We also thank Sean Markert for discussions and comments. Our observations were done with the 6-m telescope of the Special Astrophysical Observatory of the Russian Academy of Sciences. We grateful to the staff of the Observatory and specially Victor Afanasiev for his great contribution to spectroscopy at the 6-m telescope. The observations were carried out with the financial support of the Ministry of Education and Science of the Russian Federation (agreement No. 14.619.21.0004, project ID RFMEFI61914X0004). We have used the NASA/IPAC Extragalactic Database (NED) which is operated by the Jet Propulsion Laboratory, California Institute of Technology, under the contract with the National Aeronautics and Space Administration. We acknowledge the usage of the HyperLeda database (<http://leda.univ-lyon1.fr>). This work was supported by the Ministry of Education and Science of the Russian Federation (project 8523) and by the Research Program OFN-17 of the Division of Physics, Russian Academy of Sciences. AM is also grateful for the financial support of the non-profit ‘‘Dynasty’’ Foundation. AK acknowledge support of NASA and NSF grants to NMSU.

REFERENCES

- Afanasiev V. L., Moiseev A. V., 2005, *Astronomy Letters*, 31, 194
- Afanasiev V. L., Moiseev A. V., 2011, *Baltic Astronomy*, 20, 486
- Arribas S., Colina L., Bellocchi E., Maiolino R., Villar-Martín M., 2014, *A&A*, 568, A14
- Arsenault, R., Roy, J.-R. 1988, *A&A*, 201, 199
- Blasco-Herrera J., Fathi K., Beckman J. et al., 2010, *MNRAS*, 407, 2519
- Blasco-Herrera J., Fathi K., Östlin G., Font J., Beckman J. E., 2013, *MNRAS*, 435, 1958
- Bournaud F., Chapon D., Teyssier R., 2011, *ApJ*, 730, 4
- Bordalo V., Plana H., Telles E., 2009, *ApJ*, 696, 1668
- Bordalo V., Telles E., 2011, *ApJ*, 735, 52
- Burkert A., 2006, *Comptes Rendus - Physique*, 7, 433
- Cairós L. M., Vílchez J. M., González-Pérez J. N., Iglesias-Páramo J., Caon N., 2001, *ApJS*, 133, 321
- Ceverino D., Klypin A., Klimek E. S. et al., 2014, *MNRAS*, 442, 1545
- Chávez R., Terlevich E., Terlevich R. et al. 2012, *MNRAS*, 425, L56
- Chávez R., Terlevich R., Terlevich E. et al., 2014, *MNRAS*, 442, 3565
- Chu Y.-H., Kennicutt R. C. Jr., 1994, *Ap&SS*, 216, 253
- Davies R., Förster Schreiber N. M., Cresci G., et al., 2011, *ApJ*, 741, 69
- de Vaucouleurs G., de Vaucouleurs A., Corwin H. G. Jr. et al., 1991, *Third Reference Catalogue of Bright Galaxies, Version 3.9* (New York: Springer)
- Dib S., Bell E., Burkert A., 2006, *ApJ*, 638, 797
- Dopita M. A., 2008, *in Massive Stars as Cosmic Engines, Proceedings of the International Astronomical Union, IAU Symposium*, 250, 367
- Gallagher J. S., Hunter D. A., 1983, *ApJ*, 274, 141
- Genzel R., Newman S., Jones T. et al., 2011, *ApJ*, 733, 101
- Green A. W., Glazebrook K., McGregor P. J. et al., 2010, *Nature*, 467, 684
- Hippelein H. H., 1986, *A&A*, 160, 374
- Hopkins P.F., Quataert E., Murray N., 2012, *MNRAS*, 421, 3488
- Joung M. R., Mac Low M.-M., Bryan G. L., 2009, *ApJ*, 704, 137
- Kaisina, E. I., Makarov, D. I., Karachentsev I. D., Kaisin S. S., 2012, *Astrophys. Bull.*, 67, 115
- Karachentsev I. D., Karachentseva V. E., Huchtmeier W. K., Makarov D. I., 2004, *AJ*, 127, 2031
- Kennicutt Jr. R. C., 1998, *ARA&A*, 36, 189
- Kennicutt R. C. Jr., Lee J. C., Funes S. J., José G., Sakai S., Akiyama S., 2008, *ApJS*, 178, 247
- Koulouridis E., Plionis M., Chávez R. et al., 2013, *A&A*, 544, 13
- Lopez L. A., Krumholz M. R., Bolatto A. D., Prochaska J. X., Ramirez-Ruiz E., Castro D., 2014, *ApJ*, 795, 121
- Lee J. C., Gil de Paz, A., Tremonti Ch. et al. 2009, *ApJ*, 706, 599
- Mac Low M.-M., Klessen R. S., 2004, *Reviews of Modern Physics*, 76, 125
- Makarov D., Prugniel P., Terekhova N., Courtois H., Vauglin I., 2013, *MNRAS*, 428, 476
- Marino A., Plana H., Rampazzo R. et al., 2013, *MNRAS*, 428, 476
- Martínez-Delgado I., Tenorio-Tagle G., Muñoz-Tuñón C. et al., 2007, *AJ*, 133, 2892
- Melnick J., 1977, *ApJ*, 213, 15
- Melnick J., Moles M., Terlevich R., Garcia-Pelayo J.-M., 1987, *MNRAS*, 226, 849

- Melnick J., Tenorio-Tagle G., Terlevich R., 1999, MNRAS, 302, 677
- Melnick J., Terlevich R., Terlevich E., 2000, MNRAS, 311, 629
- Moiseev A.V., 2002, Bull. Spec. Astrophys. Obs. 54, 74
- Moiseev A.V., 2008, Astrophys. Bull., 63, 201
- Moiseev A.V., 2011, EAS Publications Series, 48, 115
- Moiseev A.V., 2014, Astrophys. Bull., 69, 1
- Moiseev A.V., Egorov O.V., 2008, Astrophys. Bull., 63, 181
- Moiseev A. V., Lozinskaya T. A., 2012, MNRAS, 423, 1831
- Moiseev A.V., Karachentsev I.D., Kaisin S.S., 2010a, MNRAS, 403, 1849
- Moiseev A.V., Pustilnik S. A., Kniazev A. Y., 2010b, MNRAS, 405, 2453
- Muñoz-Tuñón C., Tenorio-Tagle G., Castañeda H.O., Terlevich R., 1996, AJ, 112, 1636
- Östlin G., Amram P., Masegosa J., Bergvall N., Boulesteix J., 1999, A&AS, 137, 419
- Östlin G., Amram P., Bergvall N., Masegosa J., Boulesteix J., Márquez I., 2001, A&A, 374, 800
- Roy J.-R., Arsenault R., Joncas G., 1986, ApJ, 300, 624
- Rozas M., Zurita A., Beckman J. E., Pérez D., 2000, A&AS, 142, 259
- Scalo J., Chappell D., 1999, MNRAS, 310, 1
- Smith M. G., Weedman D. W., 1970, ApJ 161, 33
- Stilp A. M., Dalcanton J. J., Warren S. R., Skillman, E., Ott J., Koribalski B., 2013, ApJ, 765, 136
- Swinbank M., Smail I., Sobral D., Theuns T., Best Ph.n., Geach J.E., 2012, ApJ, 760, 130
- Tenorio-Tagle G., Muñoz-Tuñón C., Cox P. D, 1993, ApJ, 418 , 767
- Terlevich R., Melnick J., 1981, MNRAS, 195, 839
- Trujillo-Gomez S., Klypin A., Colín P., et al., 2015, MNRAS, 446, 1140
- Tully R. B., 1988, Nearby Galaxy Catalog, Cambridge University Press, Cambridge: 1988
- van Zee L., 2000, AJ, 119, 2757
- Vasiliev E. O., Moiseev A. V., Shchekinov Y. A., 2015, Baltic Astronomy, accepted; arXiv:1411.1269
- Voigtlaender P., Bomans D.J., Moiseev A.V., 2015, A&A, submitted.
- Wisnioski E., Glazebrook K., Blake , Ch., et al., Ch. 2012, MNRAS, 422, 3339